
YZS-MODEL: A PREDICTIVE MODEL FOR ORGANIC DRUG SOLUBILITY BASED ON GRAPH CONVOLUTIONAL NETWORKS AND TRANSFORMER-ATTENTION.

Chenxu Wang[†]
Shihezi University
Xinjing, China
zxdsama@gmail.com,
20221018267@stu.shzu.edu.cn

Haowei Ming[†]
Peking University
Beijing, China

Jian He[†]
Xinjiang University
Xinjiang, China

Yao Lu
Shihezi University
Xinjiang, China

Junhong Chen
South China University of Technology
Guangdong, China

ABSTRACT

The accurate prediction of drug molecule solubility is essential for determining their therapeutic effectiveness and safety, influencing the drug’s ADME processes. Traditional solubility prediction techniques often fail to capture the complex nature of molecular structures, leading to notable deviations between predictions and actual results. For example, the Discussion on Advanced Drug-Like Compound Structures. Lusci[1] highlighted issues in capturing crucial cyclic structural information in molecules with ring structures. To overcome this issue, our research introduces a novel deep learning framework combining attention-based transformers, Long Short-Term Memory (LSTM) networks, and Graph Convolutional Networks (GCN), aimed at enhancing the precision of solubility predictions. Utilizing a training set of 9,943 compounds and testing on an anticancer compound dataset, our method achieved a correlation coefficient (R^2) of 0.59 and a Root Mean Square Error (RMSE) of 0.57, which outperforms the benchmark models’ scores of 0.52 (R^2) and 0.61 (RMSE). Importantly, in an additional independent test, our model significantly outperformed the baseline with an RMSE of 1.05 compared to 1.28, a relative accuracy improvement of 45.9%. This research not only demonstrates the vast potential of deep learning for improving solubility prediction accuracy but also offers novel insights for drug design and selection in the future. Continued efforts will be directed towards optimizing the model architecture and extending its application to better support the drug development process, underscoring the pivotal role of deep learning in drug discovery.

1 Introduction

In contemporary medical science, the development and deployment of organic pharmaceuticals hold immeasurable value for public health improvement[2]. Organic drugs have emerged as heroes in the fight against chronic illnesses such as cancer, cardiovascular diseases, and diabetes. For example, some targeted therapies have become critical components of cancer management, markedly enhancing patient survival[3]. However, despite advancements in technology facilitating new therapeutic approaches, the path of drug development is fraught with challenges and high costs. In the U.S., the cost of bringing a new drug to market ranges from \$157.3 million to \$1.9508 billion and spans twelve to fifteen years from initial research to commercial availability[4, 5]. In this context, the precise prediction of a drug molecule’s water solubility is especially vital, as it directly influences the drug’s ADME properties, crucial for ensuring both its efficacy and safety[6].

[†] : Each symbol represented that these authors contributed equally to this work.

While traditional methods for predicting water solubility—such as empirical models (which depend on pre-existing solubility data like the Jouyban-Acree model), quantitative structure-activity relationships (QSAR) models (building mathematical models based on the analysis of physicochemical properties and biological activities of compounds), and physicochemical computational methods (utilizing simulations of molecular interactions and thermodynamic properties through computational approaches like molecular dynamics and quantum mechanics)—have shown some efficacy, as demonstrated by Munjal’s QSAR model for Paclitaxel derivatives, they frequently underperform when applied to molecules with complex structures[7, 8, 9]. Compared to machine learning techniques, the primary limitations of these traditional methods include:

1. Restricted predictive accuracy, notably for molecules that are structurally complex or exhibit novel characteristics[10];
2. A heavy reliance on extensive experimental data, limiting effectiveness in cases with few samples or novel molecular structures[11];
3. The requirement for expensive computational resources, especially in physicochemical approaches[12];
4. Insufficient comprehension of intricate molecular interactions, hindering a comprehensive reflection of molecular solubility behavior[13].

These challenges have prompted the scientific community to explore more advanced and precise methods of prediction.

Within the current pharmaceutical research landscape, deep learning provides a novel approach that significantly improves the precision and efficiency of solubility predictions. Deep learning offers distinct potential advantages over traditional methodologies:

1. **Automatic Feature Learning:** Deep learning models inherently learn and extract valuable features from complex data without relying on predefined physicochemical parameters, enabling the handling of highly complex molecular structures[14].
2. **Capacity to Handle Large Datasets:** As scientific data proliferates, deep learning adeptly manages and analyzes extensive datasets, including those derived from high-throughput experiments, which boosts the predictive model’s generalizability and accuracy[15].
3. **Adaptability and Flexibility of Models:** Deep learning models can be tailored to predict particular molecular types by modifying network structures and parameters, such as employing various neural network types like CNNs and RNNs to better process spatial and temporal molecular data[16].
4. **Swift Iteration and Updating:** Deep learning models rapidly integrate new experimental data and align with emerging research and market needs, thereby expediting the drug development timeline[17].

Therefore, deep learning is chosen as the primary predictive model due to its outstanding performance and strong adaptability to unknown or complex data, significantly expediting the drug development process and aiding in the early identification of candidates with high therapeutic potential, thus greatly reducing both cost and time in development.

Numerous studies have illustrated the role of deep learning in the fields of drug discovery and materials science. For instance, Mater et al. discussed deep learning’s applications in drug and material design and synthesis planning, underscoring its potential to enhance and expedite the drug development workflow[18]. Aliper et al. showed how deep neural networks could categorize drugs using transcriptome data, which helps predict drug effectiveness and side effects more accurately[19]. Additionally, Walters et al. applied deep learning to predict drug molecule properties, offering essential insights during the initial phases of drug design to circumvent expensive modifications during later development stages[20]. These investigations not only highlight deep learning’s impact in pharmaceutical research but also its effectiveness in tackling complex drug design challenges. Furthermore, Korotcov analyzed the performance and advantages of deep learning over other machine learning techniques in various drug discovery datasets[21]. Aliper explored predicting drugs’ pharmacological features using deep learning and discussed the prospects for drug repurposing[19]. Tang highlighted the use of deep learning in drug discovery, focusing on its potential to forecast drug-target interactions, devise new medications, and anticipate toxicities and side effects[22]. Sarode summarized deep learning techniques and their applications in drug design, including CNNs, RNNs, VAEs, and GANs[23]. Lastly, Qian et al. introduced a deep learning-based novel drug design system optimized for scenarios with limited data, utilizing one-shot and reinforcement learning to operate effectively in data-scarce environments[24].

Beyond applications in drug and materials discovery, deep learning has been widely utilized for predicting solubility in small drug molecules. For instance, Alessandro employed a novel approach using recurrent neural networks to tackle the loss of cyclic structural information[1]. Recurrent neural networks not only address this issue but also enable the automatic learning of appropriate molecular representations, decreasing the need for extensive domain expertise.

Not limited to simple RNNs, Waqar added attention mechanisms to convolutional neural networks, facilitating the broad, automatic acquisition of solubility-relevant chemical features[25]. In addition to neural network architectural innovations, Tong suggested using molecular descriptors instead of structural forms for training neural networks[26]. This approach not only simplifies the representation of complex molecular structures but also improves training efficiency. Moreover, researchers like Sumin have made innovative improvements to molecular inputs, with the MFPCP method incorporating molecular fingerprints and physicochemical properties into a combined descriptor that allows for high-performance solubility prediction[27].

In particular, to tackle unresolved challenges, this research explores and integrates cutting-edge deep learning models, ultimately innovatively utilizing a combination of Graph Convolutional Networks[28] (GCN) and Long Short-Term Memory networks[29] (LSTM), enhanced by a Transformer architecture to develop the YZS-Model. This model, which comprehends and analyzes SMILES strings, outputs predictions about the solubility of specific compounds. Our model adeptly merges multiple deep learning technologies to capture both the overall graph structure and sequential information of molecules, introducing an innovative method for predicting the solubility of drugs. The approach begins with the use of a Graph Convolutional Network (GCN) to capture the holistic graph structure of molecules, facilitating an understanding of their complex interconnections. Following this, Long Short-Term Memory networks (LSTM) and Transformer are employed to handle the sequential data within molecules. The Transformer’s self-attention mechanism is particularly effective in recognizing long-distance molecular dependencies, complemented by the LSTM’s ability to process and integrate aspects of molecular relationships not entirely captured by the Transformer[30].

This multifaceted approach, which leverages various deep learning techniques, significantly enhances the model’s ability to understand and predict molecular properties. Specifically, the use of GCN allows for a comprehensive analysis of molecular topology, capturing key structural features. The Transformer, with its robust self-attention mechanism, efficiently identifies and processes long-range dependencies within molecules. The LSTM complements the Transformer, ensuring that the model fully understands and integrates complex sequence information. This multi-technique methodology provides a fresh perspective for predicting drug solubility, demonstrating the vast potential of deep learning in chemical data analysis and pharmaceutical development.

Beyond its innovativeness, the model also performs exceptionally in benchmark tests. It achieved a coefficient of determination (R^2) of 0.55 and a root mean square error (RMSE) of 0.59 on a dataset of 62 anticancer organic drugs, clearly surpassing the existing benchmark model, AttentionFP, which scored 0.52 and 0.61 respectively. Furthermore, on a second test set compiled by Linas et al., it reached an RMSE of 1.05, significantly outperforming the benchmark model’s 1.28. This breakthrough not only validates our model’s superiority but also its high accuracy and generalization capability in practical applications.

Regarding the model’s interpretability, we conducted a two-fold feature importance analysis. The first aspect involves a quantitative ranking of the importance of features used by our model, identifying potential correlations between specific molecular features and solubility. The second aspect involves a qualitative chemical analysis of features and elements likely to have significant correlations, using the number and strength of hydrogen bonds, as well as the number of hydrophilic and hydrophobic groups and specific chemical molecules as examples. By deeply analyzing each feature and elaborating on the model’s predictive logic, we provide a solid theoretical and empirical foundation for practical applications. This assists researchers in effectively predicting and optimizing the physicochemical properties of drugs in the early stages of pharmaceutical development, thereby reducing the risk of development failures and enhancing efficiency.

In summary, this study not only showcases the immense potential of deep learning for predicting the solubility of drug molecules but also offers a new solution for reducing drug development cycles and costs[31]. As data-driven research methodologies become increasingly prevalent in drug development, we believe this marks the dawn of a new era in pharmaceutical research. We look forward to further breakthroughs in this field that could significantly contribute to human health.

2 Materials and Methods

2.1 Training and Testing

This research was conducted using a dataset gathered by Cui, Q., and colleagues, which included 9,944 organic compounds[14]. The dataset is structured with three primary components for each entry: the Simplified Molecular Input Line Entry System (SMILES), International Chemical Identifier (InChIKeys), and solubility (log S). SMILES represents molecular structures using ASCII strings, which not only streamline the electronic documentation of compounds but also enhance their computability and analytical processing. Log S, the logarithmic measure of molecular solubility in

mol/L, is determined under normal conditions at room temperature, atmospheric pressure, and a pH of 7.0, with values spanning from -18.22 to 1.70.

To assess the effectiveness of our model, three separate test sets were employed. The initial test set, curated by Waqar Ahmad et al., contained 62 clinically validated anticancer compounds, showcasing log S values between -6.52 and -2.36, with an average of -4.48 and a median of -4.46[25]. This demonstrates the diversity and experimental relevance of the dataset used. Further, we used two additional datasets released by Llinas2020 for baseline comparisons—one with 100 entries and another with 32—to thoroughly evaluate the model’s performance[32]. The distribution of log S values in other datasets is depicted in the accompanying figure 1.

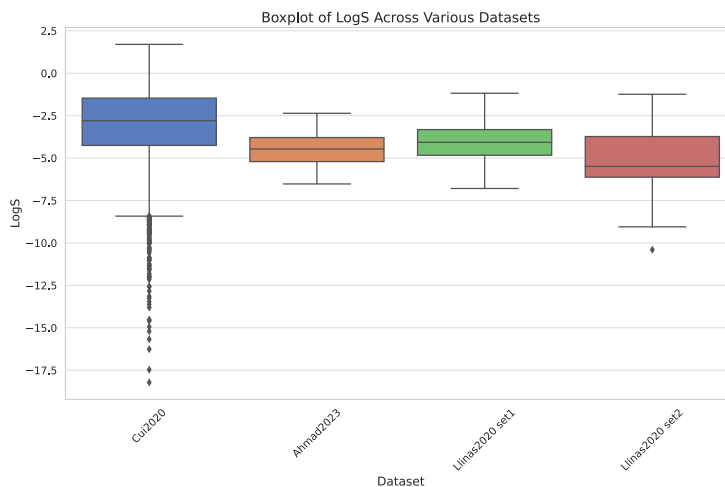


Figure 1: Solubility (log S) Distribution Across Datasets.

In terms of data handling, all datasets were standardized before being utilized for model training and testing. This preprocessing included removing duplicates, imputing missing values, and selecting relevant features. Specifically, SMILES and InChIKeys were standardized using appropriate tools to ensure consistency in the representation of compound structures. Additionally, the log S values were normalized prior to model input to mitigate the impact of numerical variations on model training.

2.2 Data Preprocessing

By employing the RDKit library, SMILES strings can be converted into molecular objects, which serve as a foundation for further extraction and analysis of molecular features. For this purpose, we constructed a feature tensor to store detailed information about each molecule’s core attributes. These features include the type of atoms, the number of bonds between atoms, formal charges on atoms, the number of free radical electrons, hybridization types, whether the atom is part of an aromatic system, the number of directly bonded hydrogen atoms, and critical information regarding chirality and stereochemistry, as detailed in Table 1. Most attributes, such as the type of elements, are represented using binary encoding—where 0 indicates absence and 1 indicates presence. A few features, like the number of directly bonded hydrogen atoms, are represented using one-hot encoding.

Regarding internal bond information of the molecules, we utilized two key data structures: ‘edge_attr’ and ‘edge_index’. ‘edge_attr’ primarily stores attributes related to the bonds, such as the type of bond (single, double, triple), whether the bond is conjugated, aromaticity, and whether the bond is part of a ring. ‘edge_index’ records the connectivity between atoms, including atom indices, type of bonds, and other relevant information, defining the structural framework of the molecule, as detailed in Table 2.

These details are subsequently integrated into a ‘torch_geometric’ Data object, which encompasses the node features, the connectivity of edges, and their attributes, thereby forming a complete graph data structure.

Table 1: Detailed Attributes of Atomic Features Utilized in Molecular Object Analysis

Atom Features	Size	Details
Symbol	66	[K, Y, V, Sm, Dy, In, Lu, Hg, Co, Mg, Cu, Rh, Hf, O, As, Ge, Au, Mo, Br, Ce, Zr, Ag, Ba, N, Cr, Sr, Fe, Gd, I, Al, B, Se, Pr, Te, Cd, Pd, Si, Zn, Pb, Sn, Cl, Mn, Cs, Na, S, Ti, Ni, Ru, Ca, Nd, W, H, Li, Sb, Bi, La, Pt, Nb, P, F, C, Re, Ta, Ir, Be, Tl]
Degree	8	Total direct connected atoms.
Formal Charge	1	Total formal charges.
Electrons	1	Total radical electrons.
Hybridization	7	s, sp, sp ² , sp ³ , sp ³ d, sp ³ d ² , other.
Aromaticity	1	Atom is in aromatic system (true/false).
Hydrogens	5	Total direct connected hydrogens.
Chirality	1	Atom is chiral (true/false).
Chirality type	2	R or S.

Table 2: Detailed Attributes of Bond Features Utilized in Molecular Object Analysis

Bond Features	Size	Details
Type	4	Single, double, triple, aromatic.
Conjugation	1	Bond is conjugate (true/false).
Ring	1	Bond is in ring (true/false).
Stereo	4	StereoNone, StereoAny, StereoZ, StereoE.

2.3 10-Fold Data Split

In our research, we adopted the version of the Cui2020 dataset segmented by Ahmad et al. for the training and testing phases of our machine learning model[25, 14]. The team led by Ahmad et al. randomly split the original Cui2020 dataset into ten equal and independent subsets, each termed a "fold." To evaluate our model’s efficacy, we implemented a 10-fold cross-validation technique: during each cycle, the model trained on nine folds and was tested on the remaining one. This procedure was replicated ten times, ensuring that each fold was used as a test set once.

This method of cross-validation enables the assessment of the model under various training-test data configurations, thereby offering a robust and credible estimate of its performance. We documented the model’s test set performance in all ten iterations, selecting the optimal model configuration for additional training and testing. The objective of this phase was to pinpoint a model configuration that provides the strongest generalization capability across the complete dataset.

2.4 Molecular Feature Extraction

Feature extraction is a pivotal component in our model. We used one-hot encoding to convert all categorical variables into binary zeros and ones. Elemental symbols were encoded into 66-bit one-hot vectors, and hybridization features were encoded using 7-bit one-hot vectors. This approach not only streamlines the handling of categorical variables by machine learning algorithms but also maintains feature independence and prevents model biases due to changes in feature ordering[33].

Utilizing the RDKit toolkit, we meticulously extracted diverse features of atoms and chemical bonds from SMILES representations of molecules and tabulated these features (refer to Tables 1 and 2). On this foundation, atoms and chemical bonds were conceptualized as nodes and edges in graph theory, respectively. These graph features were then formatted for deep learning applications using the PyG (PyTorch Geometric) library, with node features having a dimensionality of 92 and edge features having a dimensionality of 10. This comprehensive feature extraction and encoding procedure not only precisely maps the molecular structure but also equips the deep learning model with a well-suited composite description of atoms and chemical bonds.

2.5 Graph Neural Network

Graph Neural Networks (GNNs) represent a cutting-edge deep learning framework, devised for processing and predicting data that takes the form of graphs. In contrast to conventional deep learning models, GNNs adeptly manage datasets with complex interrelations and varying dimensions, thus exhibiting exceptional utility in numerous domains. GNNs function by precisely modeling the interactions among nodes and edges in a graph, thereby learning and extracting profound characteristics of graph data. In this framework, each node signifies an entity, while edges represent the relationships among these entities. The unique aspect of GNNs lies in their iterative process of updating node states, which enhances node representations by leveraging information from adjacent nodes. The input for a GNN consists of an undirected graph G .

$$G = (V, E) \quad (1)$$

Here, V denotes the set of all nodes within the graph, and E refers to the collection of edges that directly connect the nodes. Each node $v \in V$ is associated with an initial feature vector x_v , encoding both node and edge characteristics. The objective of a GNN is to devise a function f that produces a sophisticated feature representation h_v for every node, capable of encapsulating both the local structural dynamics and the intricate interactions of node features.

In the case of node v , updating its hidden state each round consists of the following steps:

1. **Message Passing:** First, compute the message passed to node v from each of its neighboring nodes $u \in N(v)$ using the equation:

$$m_{uv}^{(t+1)} = M(h_v^{(t)}, h_u^{(t)}, x_u, x_v, e_{uv}) \quad (2)$$

where M stands for the message function, $h_v^{(t)}$ and $h_u^{(t)}$ are the hidden states of nodes v and u in iteration t , x_v and x_u are the nodes' initial features, and e_{uv} is the feature of the edge connecting v and u .

2. **Aggregation:** Node v aggregates the messages received from all its neighbors into a single composite message using:

$$a_v^{(t+1)} = A(\{m_{uv}^{(t+1)} : u \in N(v)\}) \quad (3)$$

A represents the aggregation function, which may be summing, averaging, or taking the maximum value.

3. **State Update:** Finally, the hidden state of node v is updated with the update function:

$$h_v^{(t+1)} = U(h_v^{(t)}, a_v^{(t+1)}, x_v) \quad (4)$$

U denotes the update function, which could be a straightforward linear transformation with a nonlinear activation or a more intricate neural network.

These procedures allow GNNs to iteratively update the hidden states of each node in the graph. Eventually, the hidden states converge, encapsulating and reflecting the features of their neighboring nodes and the graph's structural properties. This iterative cycle is generally repeated for several rounds until the nodes' hidden states stabilize or reach the pre-set number of iterations.

The output of a GNN is tailored to fit specific tasks such as node classification, graph classification, or link prediction. In the case of node classification, the network maps the final hidden state $h_v^{(T)}$ of a node to its predicted label using a readout layer R :

$$\hat{y}_v = R(h_v^{(T)}) \quad (5)$$

where T denotes the total number of iteration rounds completed, and \hat{y}_v represents the predicted label for node v . This approach allows the GNN to deduce the label of each node by integrating information from its features and neighborhood over multiple iterations.

2.6 Graph Convolution Network

In our research, we introduced a single-layer Graph Convolutional Network (GCN) architecture to handle graph data. This GCN utilizes convolution operations on the graph structure to adeptly capture the relationships between the features of nodes and their adjacent neighbors. In our model, the GCN layer principally serves to transform node features from 92 dimensions to 128 dimensions, thus augmenting their representational power. Through this approach, the GCN layer not only enhances our comprehension of the nodes' local structures but also provides a higher-dimensional feature representation to facilitate the analysis of complex interactions within the graph data, strongly supporting subsequent analytical and predictive endeavors[34].

2.7 Self-Attention Transformer

In our research, we utilized a Self-Attention Transformer architecture designed to analyze and predict the solubility of organic drugs. This architecture differs from conventional deep learning models such as RNNs and LSTMs by employing a self-attention mechanism that captures global dependencies within sequences. This feature significantly improves the model’s capability to process long-distance dependencies[35].

The self-attention mechanism enables the model to focus on any position within the sequence, calculating representations for each position and dynamically adjusting its focus to detect long-range dependencies. For an input sequence representation $X \in \mathbb{R}^{n \times d}$ where n is the length of the sequence and d is the dimension of features, the self-attention layer computes attention scores for each element in relation to others, expressed as:

$$\text{Attention}(Q, K, V) = \text{softmax}\left(\frac{QK'}{\sqrt{d_k}}\right) V \quad (6)$$

In this formula, Q , K , and V denote the query, key, and value matrices, respectively, derived by multiplying the input sequence X with corresponding weight matrices; d_k stands for the dimension of the key vectors.

The Transformer architecture is built from encoder and decoder components, consisting of several repeating layers. Each layer includes a multi-head self-attention mechanism and a position-wise fully connected feed-forward network, both supplemented by residual connections and layer normalization, as illustrated in Figure 2.

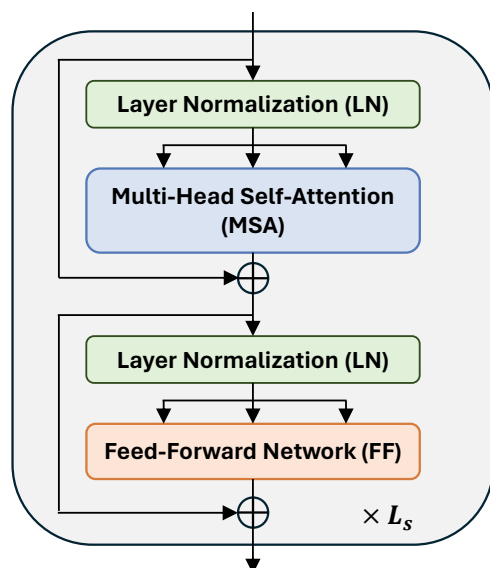


Figure 2: An overview of the Transformer model structure, LN, MSA, and FF, demonstrates critical steps in sequence data processing.

1. **Multi-Head Self-Attention:** This component comprises parallel-executed self-attention layers, enabling the model to capture diverse information across multiple subspaces, thereby enhancing its capability to represent various features.
2. **Feed-Forward Network:** Each position’s feature vector undergoes two linear transformations and a nonlinear activation within this network, promoting further information synthesis.

In the context of predicting drug solubility, the Transformer leverages feature vectors refined by graph convolutional networks to understand the interactions among atoms and functional groups within a molecule’s neighborhood.

2.8 Long Short-term Memory

In our research, Long Short-Term Memory (LSTM) networks have been utilized to enhance the analysis and prediction of organic drug solubility. LSTMs, advanced variants of Recurrent Neural Networks designed to capture long-term

dependencies in sequence data, are particularly tailored in this study to optimize outputs derived from Self-Attention Transformer architectures, revealing deeper sequential dependencies in molecular sequences.

LSTMs effectively solve the gradient vanishing or exploding problems seen in traditional RNNs when handling long sequences, thanks to their distinctive gating mechanism. This includes:

1. **Forget Gate:** It assesses which information should be removed from the cell state, based on the current input and the previous hidden state.
2. **Input Gate:** It decides which new information is to be incorporated into the cell state.
3. **Output Gate:** It determines what the next hidden state should be, computed from the current cell state influenced by the gates' outputs.

Thus, by handling the outputs from the Self-Attention Transformer, the LSTM not only bolsters the model's grasp of sequence dependencies but also robustly supports precise predictions of solubility in organic drugs. This method allows us to exploit complex interactions within drug molecular structure sequences, providing more detailed and accurate feature representations for predicting solubility.

2.9 YZS-Model

In this study, we introduced the YZS-Model, which aims to precisely predict the solubility of organic drugs. This model combines Graph Convolutional Networks (GCN), Transformer architecture, and Long Short-Term Memory networks (LSTM) to thoroughly investigate the spatial structure and sequence dynamics of drug molecules, as illustrated in Figure 3.

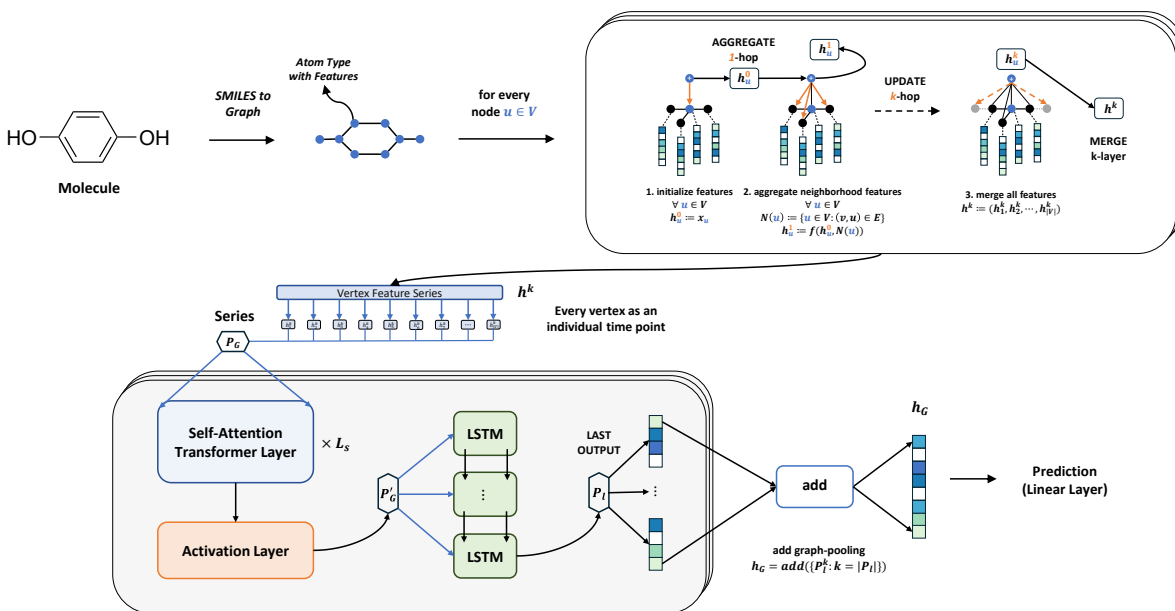


Figure 3: Architecture of the YZS-Model. Initially, drug molecules are converted from SMILES notation into a graph representation, with each atom encoded as a node and bonds as edges. Features are aggregated through a Graph Convolutional Network (GCN) to capture structural information. Subsequently, these features are processed by a self-attention Transformer layer to capture global dependencies. The sequence dynamics are then analyzed via an LSTM layer. Finally, graph pooling and Linear Layer are used to output solubility predictions.

The model begins by employing a GCN to process the graphical representation of drug molecules, effectively unveiling their spatial structure. The GCN layer abstracts intricate feature vectors that describe molecular topologies by analyzing interactions between molecular atoms and their chemical bonds, providing a robust foundation for detailed structural analysis.

The model then utilizes the Transformer architecture to enhance the feature output from the GCN layer. Utilizing self-attention, the Transformer discerns broad dependencies among atoms within the molecule, capturing both mi-

crostructural details and comprehensive internal interactions, thus offering an advanced representation enriched with global information.

The LSTM layer further refines the understanding of features produced by the Transformer, capturing temporal dependencies inherent in the molecular structure sequences. This step is pivotal for uncovering the dynamic nature of molecular features across sequences, thereby enriching the solubility predictions with temporal insights.

Ultimately, the model’s fully connected layers transform the LSTM outputs into final solubility predictions, synthesizing high-dimensional features from the GCN, Transformer, and LSTM, and associating these features with the drug molecules’ solubility through nonlinear transformations. The design of the entire model is focused on effectively translating the spatial and temporal characteristics of molecules into their solubility properties, thus ensuring high precision and reliability in the solubility predictions for organic drugs.

2.10 Implementation Details

In our research, we focused on optimizing the hyperparameters of the YZS-Model to improve its predictive accuracy for the solubility of organic drugs. Using the hyperopt library and the Tree-structured Parzen Estimator (TPE) algorithm, we conducted a systematic exploration and evaluation of several critical hyperparameters, such as learning rate, dimensions of feature vectors, Dropout rate, depth of Transformer layers, number of heads in the multi-head self-attention, and batch size, to discover the best model configuration[36]. The hyperopt training was configured to stop after 200 iterations, with the details documented in a log file, as illustrated in the provided Table 3.

Table 3: Detailed YZS-model hyperopt training parameters

Item	Range	Selection method
lr	(0.0003,0.0007)	hp.uniform
dim	(92,128,2)	hp.quniform
dropout	(0.25,0.35)	hp.uniform
depth	[2,4,6,8,12]	hp.choice
heads	[4,8,12,16]	hp.choice
batch_size	(24,72,8)	hp.quniform

We ultimately set the depth of the Transformer layers to six, with each layer having eight heads with a dimension of 92, and an Linear Layer dimension of 256, while setting the Dropout rate to 0.25. For the YZS-Model, the number of input features was adjusted to 92, with the feature dimensions increased to 128 and the Dropout rate finely adjusted to 0.2519. These precise modifications, underpinned by rigorous experimental and validation efforts, markedly enhanced the YZS-Model’s performance in predicting solubility.

2.11 Evaluation Metrics

In our research, the model’s performance is assessed using two key metrics: the coefficient of determination (R^2) and the Root Mean Square Error (RMSE).

Coefficient of Determination (R^2): This metric measures the goodness of fit of the model to the observed data. It reflects the model’s ability to explain the variability of the dependent variable, with values ranging from 0 to 1. A higher R^2 value indicates a better fit. It is computed as follows:

$$R^2 = 1 - \frac{\sum_{i=1}^n (y_i - \hat{y}_i)^2}{\sum_{i=1}^n (y_i - \bar{y})^2} \quad (7)$$

Where y_i is the actual value, \hat{y}_i is the model’s prediction, \bar{y} is the average of the actual values, and n is the sample size.

Root Mean Square Error (RMSE): RMSE quantifies the model’s prediction accuracy by calculating the square root of the average of the squared discrepancies between the actual and predicted values. A smaller RMSE value indicates greater accuracy. Its formula is:

$$\text{RMSE} = \sqrt{\frac{1}{n} \sum_{i=1}^n (y_i - \hat{y}_i)^2} \quad (8)$$

Both metrics offer a method to quantitatively assess and delve into the model’s efficacy in predicting the solubility of organic drugs.

3 Results and Discussion

3.1 Performance of YZS-Model

In our research, two metrics were employed to thoroughly evaluate the performance of the proposed model: the coefficient of determination (R^2) and the Root Mean Square Error (RMSE). The R^2 index measures the model’s ability to explain data variability, whereas RMSE assesses the deviations between predicted and actual values. The YZS-Model was evaluated using a ten-fold version of Cui, Q.’s dataset partitioned by Ahmad et al., with Ahmad’s AttentiveFP model used as a comparative baseline. Training results shown in Table 3 reveal that our YZS-Model surpasses the baseline model, reaching peak performance.

Further validation was conducted using a dataset of 62 anticancer compounds compiled by Ahmad, as displayed in Table 4. The outcomes indicate that the YZS-Model attained scores of 0.59 in RMSE and 0.55 in R^2 , substantially outperforming the baseline AttentiveFP model’s scores of 0.61 and 0.52 and other traditional models, underscoring our model’s superior performance.

Table 4: AttentiveFP Dataset Results Comparison

Model	R^2	RMSE
GIN-based GNN	0.21	0.78
SGConv-based GNN	0.09	1.98
GAT-based	0.38	0.69
14 layers ResNet	0.13	0.82
20 layers ResNet	0.41	0.68
26 layers ResNet	0.07	0.85
AttentiveFP-based GNN	0.52	0.61
YZS-Model	0.59	0.57

Furthermore, our research also utilized the dataset by Llinas et al. (2020) for additional model evaluation. Importantly, although the YZS-Model did not perform as expected on the test set1, it showed outstanding results on set2, with an RMSE of 1.05. This significantly outperforms the baseline model, AttentiveFP, which scored 1.28, and the SolTransNet model, which scored 1.24, as shown in Table 5. These results substantiate the model’s effectiveness and potential for application.

Table 5: SolTransNet Test Dataset Results Comparison

Test set model	RMSE	
	Llinas2020 set1	Llinas2020 set2
SolTransNet	0.95	1.24
AttentiveFP-based GNN	0.92	1.28
YZS-Model	0.98	1.05

Error analysis is depicted in Figure 4, which shows the error probability distribution. This distribution plots the difference between the predicted logarithmic solubility values (\hat{y}) and the actual logarithmic solubility values (y) of the test molecules. With an error mean of 0.07, the figure highlights the average error level across the entire test set, visually demonstrating the distribution of errors within various ranges, with the majority of errors concentrated around the mean and larger errors being less frequent.

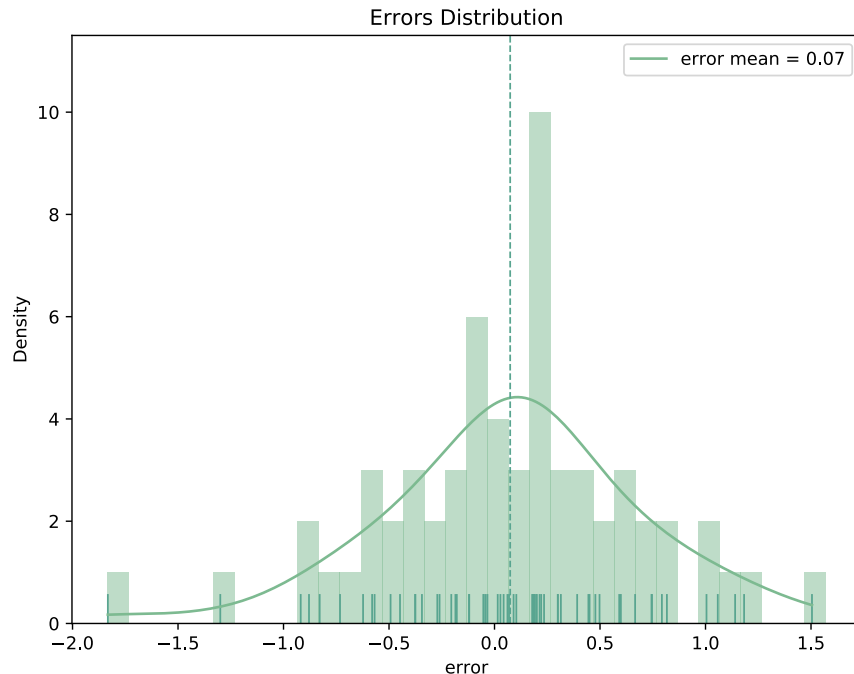


Figure 4: Error probability distribution of the YZS-Model on the test dataset.

3.2 Interpretative Analysis of YZS-Model

In our model interpretation, we utilized the random feature zeroing technique to explore how atomic features influence the prediction biases for chemical molecules. Given that we employ one-hot encoding for the 66 elements, we chose to separately rank the atomic differences from other features. This separation enables a more accurate evaluation of each component’s individual contribution to the prediction deviations.

For the calculation of differences via random zeroing, we used an averaging approach—taking the average of a feature and its sub-features as the representative value for the entire feature. This method aims to consolidate the data from each sub-feature to more fully demonstrate the collective role of each feature and the one-hot encoded atoms in the model’s prediction performance. The effects of this method, both in terms of quantification and qualitative analysis, are clearly illustrated in Figure 5 and detailed in the subsequent text.

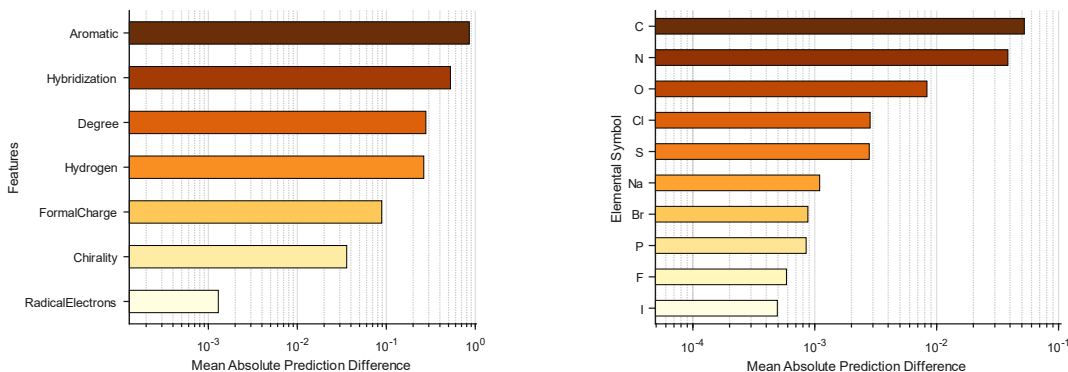


Figure 5: Ranking of Feature Importance using the Random Zeroing Method.

In our research, we applied the technique of random feature zeroing to investigate the specific impacts of atomic features on prediction deviations for chemical molecules. Besides the element type, four features notably influenced predictions: aromaticity, hybridization type, the number of other atoms directly connected, and the number of directly connected

hydrogens. Lesser influences were observed from features such as formal charge and stereoisomerism. Consequently, our primary analysis focused on these four features, with their importance indices detailed below:

Table 6: Mean Absolute Prediction Difference Index of Features

Feature	MAPD
Aromatic	0.8563
Hybridization	0.5253
Degree	0.2781
Hydrogen	0.2636

Aromaticity proved to have a significant impact on the model's solubility predictions, which was unexpected. This influence might stem from how aromatic rings alter molecular interactions and electronic structures, as depicted in Figure 6[37, 38]. Traditional solubility theories suggest that factors like polarity magnitude, number and strength

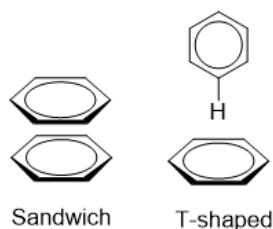


Figure 6: Aromatic rings' influence on molecular forces and electronic structures.

of hydrogen bonds, and the balance of hydrophilic and hydrophobic groups primarily affect solubility (illustrated in Figure 7)[39]. From these theories, we hypothesize that aromaticity's effect could be explained by the presence of

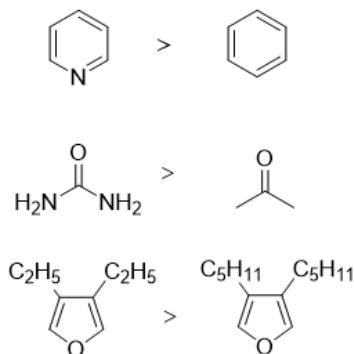


Figure 7: Solubility comparison among similar organic substances.

benzene rings and other aromatic structures which might indicate lower polarity and thus, reduced solubility[40]. These rings also introduce significant hydrophobicity, whereas heteroaromatic rings, generally polar, can increase solubility, like pyridine which acts as a hydrogen bond donor (shown in Figure 8). This suggests that aromaticity's influence on solubility is complex, shaped by multiple overlapping factors. The requirement for specific hybridization (sp^2) on aromatic ring atoms further suggests a substantial role for hybridization in the predictions. The number of connected atoms, while related to atom type and hybridization, is less directly connected to aromaticity, possibly due to the diversity of atom types like C, N, O, etc. The number of connected hydrogens might relate to polarity and hydrophobic or hydrophilic nature, whereas connections to other atoms could complexly affect these properties, directly impacting solubility. Further experimental design is needed to explore these hypotheses.

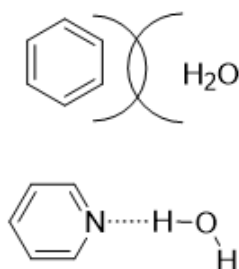


Figure 8: Diagram of benzene and pyridine interactions with water.

Besides the explanations provided earlier, we also utilized the LIME technique to rank individual features by their importance and displayed the top 15 features as shown below Figure 9. The sign on the x-axis represents whether the effect of the feature on solubility is positive (blue) or negative, where positive values indicate an increase in solubility, and negative values denote a decrease. The magnitude of the effect on solubility is depicted by the absolute value on the x-axis, with larger values representing a more significant impact. The y-axis illustrates the conditions under which each feature exerts its effect. For example, a positive score for "No Br" indicates that the absence of Br in an organic compound enhances solubility.

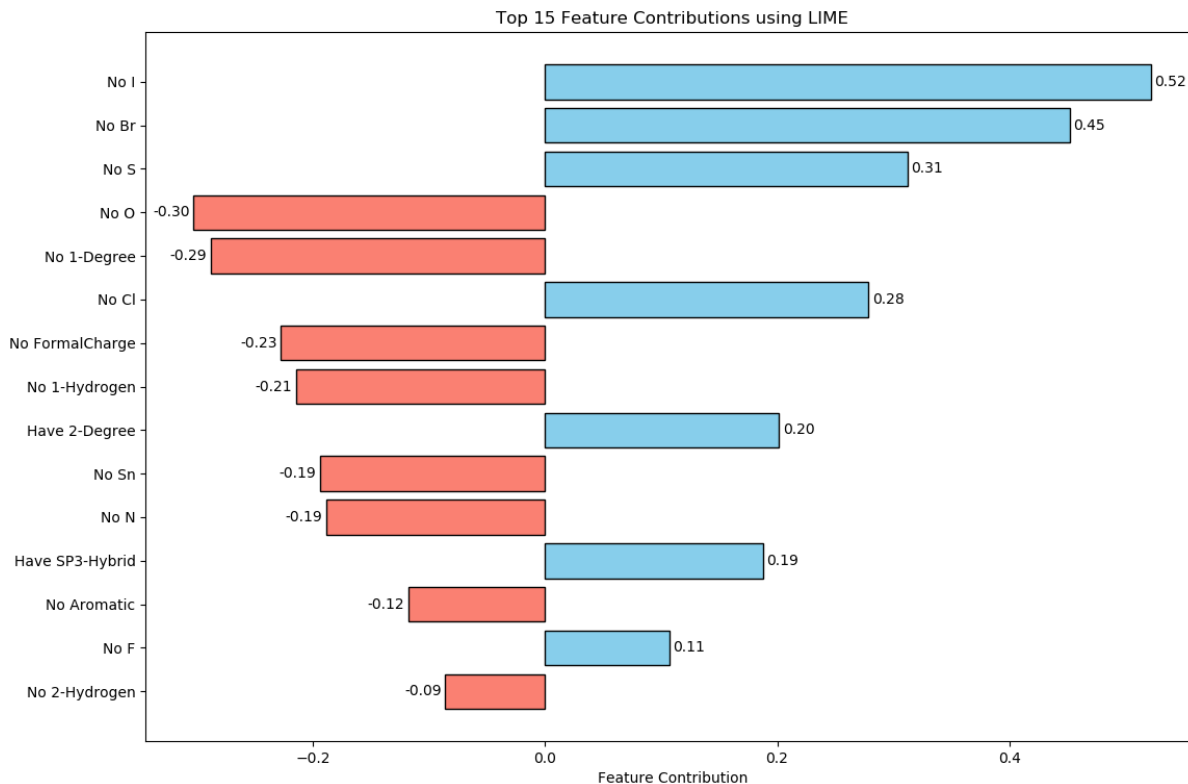


Figure 9: Ranking of individual features obtained via LIME, with red indicating negative influence and blue indicating positive influence.

Figure 9 clearly shows that LIME identifies halogen atoms (F, Cl, Br, I, etc.) as having a substantial effect on molecular solubility. The lack of these atoms significantly increases solubility. Moreover, other factors with notable influence on

the model's solubility predictions include the presence of S, N, and O, the degree of atom connectivity, the presence of formal charges, and the number of hydrogen atoms attached to an atom, along with hybridization and aromatic properties. These properties are categorized as follows: atom types, molecular complexity, and structural characteristics.

Atom Types and Their Impact on Solubility: In general, organic compounds with lower polarity exhibit lower solubility. LIME's results demonstrate that atom types significantly affect solubility. Halogen atoms reduce intermolecular polar interactions, decreasing solubility. In contrast, elements like S, N, and O form polar functional groups that increase molecular polarity and thus solubility. For example: Hydroxyl (-OH): Forms hydrogen bonds with water, significantly enhancing solubility. Amino (-NH₂) or Amide (-CONH₂): These functional groups are highly electronegative, improving solubility. Non-polar functional groups like thioether: Sulfur reduces molecular polarity, leading to lower solubility[41].

Molecular Complexity and Connectivity: **Formal Charge:** The presence of formal charges generally increases molecular polarity, thus enhancing solubility. **Degree of Connectivity:** Higher connectivity indicates more complex molecular structures. For instance, more hydrogen atoms can increase hydrophobicity, affecting solubility[42].

Structural Properties: **Aromaticity:** Aromatic rings with polar functional groups (e.g., hydroxyl, carboxyl, or amino groups) can enhance solubility through hydrogen bonding with water. **Hybridization (sp² vs. sp³):** Sp³ hybridization tends to form more complex, non-planar structures compared to sp², increasing intermolecular voids and potential polar interactions, thus improving solubility[43].

To validate LIME's importance index, we predicted the solubility of pyridine and benzene. This involved calculating the top 15 solubility indices for these compounds to qualitatively assess solubility. As illustrated in Figure 10, the YZS-model compared the solubility of benzene and pyridine: **Impact of Atom Types:** Benzene lacks the N element found in pyridine, leading to a solubility index 0.19 lower according to LIME. **Degree of Connectivity:** Pyridine's N atom is connected to two atoms, whereas benzene's corresponding position connects to three, resulting in a solubility index 0.20 lower for benzene. **Other Factors:** The compounds are otherwise identical, so no further analysis is needed. Ultimately, pyridine's solubility index is 0.39 higher than benzene's, consistent with actual solubility observations.

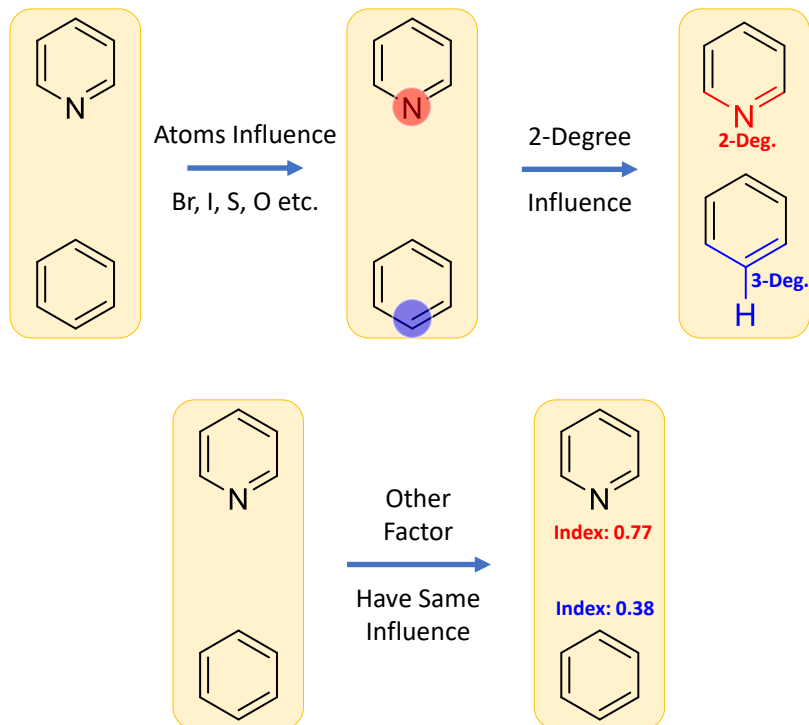


Figure 10: Qualitative solubility comparison between benzene and pyridine based on rankings provided by LIME.

3.3 Ablation experiment for YZS-Model

In an effort to better understand the sources of the interpretability performance of the YZS-Model, we carried out a series of ablation experiments. Ablation experiments operate by sequentially controlling individual conditions or parameters and observing the resulting performance changes, thereby identifying the contributions of various model components to the overall performance. To explore the model’s dependency on the training dataset, we began by randomly shuffling the dataset and then splitting it into 25%, 50%, and 75% portions of the original dataset size. We trained the model using these subsets, and the results are illustrated in Figure 11.

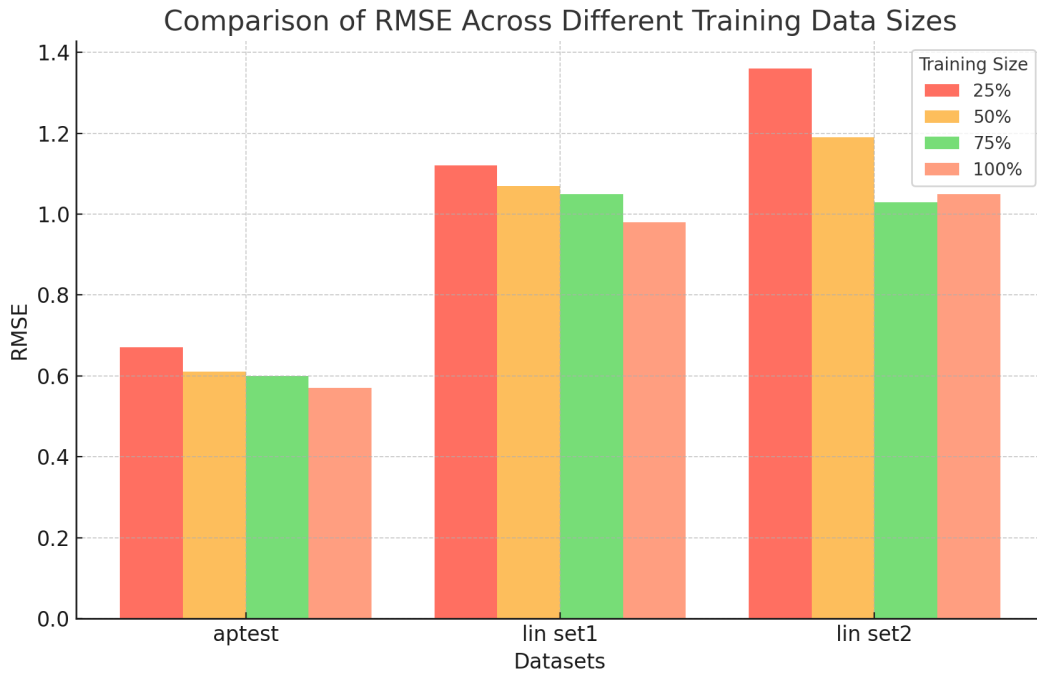


Figure 11: .

As illustrated in Figure 10, the model’s performance is less than satisfactory when trained on only 25% of the original dataset. Nevertheless, a substantial improvement in prediction accuracy is observed when the training set is increased to 50%. Further expansion of the training data to 75% and 100% results in continued performance enhancement, though the improvement plateaus beyond the 75% threshold. This demonstrates that our model effectively utilizes training data, achieving baseline performance with just half of the original dataset.

To gain further insights into the contributions of different modules of the YZS-Model during prediction, we performed a series of combinatorial module ablation experiments. We systematically combined the three crucial sub-modules in various ways and conducted ablation tests on these configurations. This approach allows us to evaluate the impact of each module on the prediction accuracy, thereby deepening our understanding of the model. The results of these experiments are illustrated in Figure 11.

Firstly, we examined the impact of ablating individual modules. By removing the GCN, Transformer, and LSTM modules separately, we observed that eliminating the GCN module had minimal effect on prediction performance, while the removal of the Transformer and LSTM modules resulted in significant performance degradation. Further analysis of dual module ablation experiments revealed that the model achieved optimal performance when both GCN and LSTM were removed, highlighting the substantial positive influence of the Transformer module on prediction results. This finding is corroborated by additional dual module ablation experiments: prediction performance markedly declines when either LSTM or GCN is retained without the Transformer. Thus, we conclude that the Transformer is the critical predictive module in the YZS-Model.

To investigate further the impact of the Transformer’s internal components on prediction results, we performed two sets of ablation experiments. Firstly, we replaced the Transformer’s key components, including the Multi-Head Self-

Attention (MSA) mechanism and the Feed-Forward Network (FFN), with identity mappings. Secondly, we conducted a series of ablation experiments to examine how varying the number of layers within the Transformer’s internal components affects prediction performance. The experimental results are shown in Figure 12.

In the first set of experiments, replacing MSA or FFN with identity mappings resulted in a significant increase in RMSE, underscoring the importance of these components to the Transformer. In the second set of layer ablation experiments, RMSE exhibited a trend of initially decreasing and then increasing. We hypothesize that with fewer layers, the Transformer struggles to capture the decisive factors in the data effectively; whereas, with more layers, the complexity of the structure may lead to overfitting, thus increasing RMSE. Notably, although the model performed best with 12 layers on the set2 dataset, its performance was inconsistent across other test sets. We attribute this to the inherent randomness in the training process. Taking all factors into account, we conclude that a 6-layer Transformer is the most appropriate structure for this task.

These experimental findings provide valuable insights into the contributions of each component of the YZS-Model in prediction tasks and offer a foundation for further optimization of the model. Through these ablation experiments, we not only confirmed the critical role of the Transformer module but also revealed the specific impacts of its internal components and layer configurations on model performance, thereby guiding future research and applications.

3.4 Discussion

This research highlights the critical role of considering specific molecular structural features during the design and training stages of the model, as well as the necessity for specifically optimizing these features to improve model performance. Future initiatives will aim to enhance the model’s adaptability and precision in predicting rare molecular structures, ensuring superior results across a more extensive dataset range.

Although the YZS-Model exhibited excellent performance across most testing datasets, its performance on the Llinas2020 set1 did not reach the anticipated levels and failed to exceed existing benchmark models. This observation suggests that the Llinas2020 set1 dataset might include unique molecular structures that are seldom present in the training set, which hinders the model’s ability to learn their essential features fully. Moreover, despite the theoretical capability of the GCN and Transformer mechanism to effectively identify complex structures and long-range dependencies, the model exhibits certain limitations when dealing with very rare molecular structures.

Further insights are provided by an in-depth analysis of the NumHAcceptors distribution. The Llinas2020 set1 contains more molecules with a high number of hydrogen bond acceptors compared to the training and other test sets, as depicted in Figure 12, potentially explaining the model’s poor performance on this particular dataset.

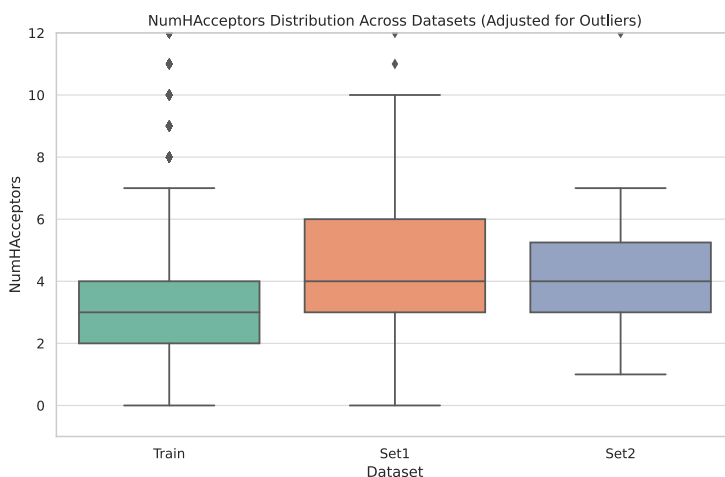


Figure 12: Potential differences in the number of hydrogen bond acceptors in the Set1 dataset.

Furthermore, our analysis suggests that the model’s performance discrepancies across different datasets could also be attributed to the number of functional groups in the molecules. Molecules with more functional groups are inherently more complex, increasing the likelihood of feature loss during the feature aggregation phase. Notably, the data distribution of the Llinas2020 set2 test dataset shows high similarity to our training dataset sourced from Cui, Q.

However, a significant difference exists with Llinas2020 set1, and we hypothesize that the unusual complexity of Set1 could be a critical factor affecting prediction outcomes.

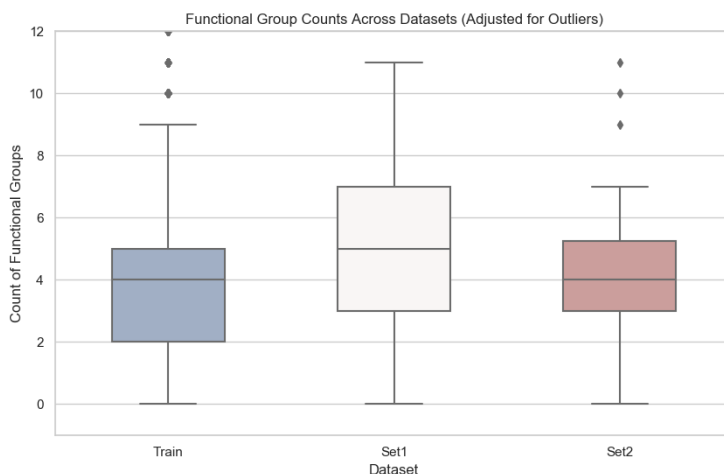


Figure 13: Potential differences in the number of functional groups (complexity) in the Set1 dataset.

Our study reveals further potential limitations of the model, especially when processing molecules with specific and rare structural traits or complex features, where there is room for improvement in prediction accuracy. Future research could enhance model generalization by incorporating a more varied range of datasets or by implementing more sophisticated feature extraction and learning methods to refine model performance.

Significantly, our model shows extensive potential for application in drug design and development. Precise solubility predictions in high-throughput screening can assist researchers in more effectively identifying and optimizing potential drug candidates, thus speeding up the drug development pipeline and lowering costs. Additionally, the accuracy and generalization capabilities of the YZS-Model offer novel insights into the intricate connections between molecular structures and their physicochemical properties.

4 Conclusion

This research introduces and validates the YZS-Model, a novel deep learning framework that incorporates Graph Convolutional Networks (GCNs), Transformer architectures, and Long Short-Term Memory networks (LSTMs) for accurate solubility prediction of organic drugs. This integration allows the YZS-Model to comprehensively analyze the molecular spatial structures and sequence dynamics, significantly enhancing its predictive performance.

The model has shown superior performance on diverse test sets, particularly excelling in the solubility predictions of anticancer compounds, outperforming existing benchmarks. Moreover, our detailed analyses of feature importance have unveiled critical factors affecting solubility, offering insights crucial for drug design and optimization.

Despite its successes, the model's performance on molecules with unique and rare structures suggests areas for improvement. Future studies will aim to extend the model's framework to include techniques such as semi-supervised and unsupervised learning, utilizing unlabeled data to better generalize to unknown datasets.

In summary, the YZS-Model not only showcases its strong potential in solubility prediction but also opens new avenues for deploying deep learning in drug discovery and development. Such technologies could potentially assist in preclinical drug screening and optimizing candidate drugs to enhance bioavailability. Furthermore, they hold promise for integrating personalized genetic information to predict drug responses, thereby informing personalized treatment strategies. We anticipate future endeavors to further explore and extend these innovative technologies to contribute significantly to human health.

Despite our achievements, it is vital to acknowledge that drug development involves a wide array of complex factors beyond the explanatory power of a single model. Therefore, ongoing exploration and enhancement by future researchers are essential to fully exploit the extensive capabilities of deep learning in drug development.

Acknowledgments

There are no conflicts to declare.

References

- [1] Alessandro Lusci, Gianluca Pollastri, and Pierre Baldi. Deep architectures and deep learning in chemoinformatics: the prediction of aqueous solubility for drug-like molecules. *Journal of chemical information and modeling*, 53(7):1563–1575, 2013.
- [2] Young-Won Chin, Marcy J Balunas, Hee Byung Chai, and A Douglas Kinghorn. Drug discovery from natural sources. *The AAPS journal*, 8:E239–E253, 2006.
- [3] Anne V Soerensen, Frede Donskov, Gregers G Hermann, Niels V Jensen, Astrid Petersen, Henrik Spliid, Rickard Sandin, Kirsten Fode, and Poul F Geertsen. Improved overall survival after implementation of targeted therapy for patients with metastatic renal cell carcinoma: results from the danish renal cancer group (darenca) study-2. *European Journal of Cancer*, 50(3):553–562, 2014.
- [4] Vinay Prasad and Sham Mailankody. Research and development spending to bring a single cancer drug to market and revenues after approval. *JAMA internal medicine*, 177(11):1569–1575, 2017.
- [5] V Veljkovic, N Veljkovic, JA Esté, A Huther, and U Dietrich. Application of the eiip/ism bioinformatics concept in development of new drugs. *Current medicinal chemistry*, 14(4):441–453, 2007.
- [6] Can Sarisozen, Ujjwal Joshi, Livia Palmerston Mendes, and Vladimir P Torchilin. Stimuli-responsive polymeric micelles for extracellular and intracellular drug delivery. In *Stimuli Responsive Polymeric Nanocarriers for Drug Delivery Applications*, pages 269–304. Elsevier, 2019.
- [7] J Taskinen. Prediction of aqueous solubility in drug design. *Current Opinion in Drug Discovery & Development*, 3(1):102–107, 2000.
- [8] Abolghasem Jouyban. In silico prediction of drug solubility in water-ethanol mixtures using jouyban-acree model. *J. Pharm. Pharm. Sci*, 9(2):262–269, 2006.
- [9] Pablo R Duchowicz, Alan Talevi, Luis E Bruno-Blanch, and Eduardo A Castro. New qspr study for the prediction of aqueous solubility of drug-like compounds. *Bioorganic & Medicinal Chemistry*, 16(17):7944–7955, 2008.
- [10] William L Jorgensen and Erin M Duffy. Prediction of drug solubility from structure. *Advanced drug delivery reviews*, 54(3):355–366, 2002.
- [11] Christopher A Lipinski, Franco Lombardo, Beryl W Dominy, and Paul J Feeney. Experimental and computational approaches to estimate solubility and permeability in drug discovery and development settings. *Advanced drug delivery reviews*, 23(1-3):3–25, 1997.
- [12] Sina Dadmand, Farzin Kamari, William E Acree, and Abolghasem Jouyban. Solubility prediction of drugs in binary solvent mixtures at various temperatures using a minimum number of experimental data points. *AAPS PharmSciTech*, 20:1–11, 2019.
- [13] Christopher, A. Lipinski, Beryl, W. Dominy, Paul, and J. Feeney. Experimental and computational approaches to estimate solubility and permeability in drug discovery and development settings. *Advanced drug delivery reviews*, 46 1-3:3–26, 2001.
- [14] Qiuji Cui, Shuai Lu, Bingwei Ni, Xian Zeng, Ying Tan, Ya Dong Chen, and Hongping Zhao. Improved prediction of aqueous solubility of novel compounds by going deeper with deep learning. *Frontiers in oncology*, 10:121, 2020.
- [15] Mohammad M Ghahremanpour, Anastasia Saar, Julian Tirado-Rives, and William L Jorgensen. Ensemble geometric deep learning of aqueous solubility. *Journal of Chemical Information and Modeling*, 63(23):7338–7349, 2023.
- [16] Peng Gao, Jie Zhang, Yuzhu Sun, and Jianguo Yu. Accurate predictions of aqueous solubility of drug molecules via the multilevel graph convolutional network (mgcn) and schnet architectures. *Physical Chemistry Chemical Physics*, 22(41):23766–23772, 2020.
- [17] Jianping Liu, Xiujuan Lei, Chunyan Ji, and Yi Pan. Fragment-pair based drug molecule solubility prediction through attention mechanism. *Frontiers in Pharmacology*, 14:1255181, 2023.
- [18] Adam C Mater and Michelle L Coote. Deep learning in chemistry. *Journal of chemical information and modeling*, 59(6):2545–2559, 2019.

- [19] Alexander Aliper, Sergey Plis, Artem Artemov, Alvaro Ulloa, Polina Mamoshina, and Alex Zhavoronkov. Deep learning applications for predicting pharmacological properties of drugs and drug repurposing using transcriptomic data. *Molecular pharmaceutics*, 13(7):2524–2530, 2016.
- [20] W Patrick Walters and Regina Barzilay. Applications of deep learning in molecule generation and molecular property prediction. *Accounts of chemical research*, 54(2):263–270, 2020.
- [21] Alexandru Korotcov, Valery Tkachenko, Daniel P Russo, and Sean Ekins. Comparison of deep learning with multiple machine learning methods and metrics using diverse drug discovery data sets. *Molecular pharmaceutics*, 14(12):4462–4475, 2017.
- [22] Yuxuan Tang. Deep learning in drug discovery: applications and limitations. *Frontiers in Computing and Intelligent Systems*, 3(2):118–123, 2023.
- [23] Ketan Dinkar Sarode. Applications of deep learning in drug discovery. *Advances in Bioengineering*, pages 73–91, 2020.
- [24] Yuchen Qian, Yuan Xing, and Liang Dong. Deep learning for a low-data drug design system. In *2020 IEEE International Conference on E-health Networking, Application & Services (HEALTHCOM)*, pages 1–4. IEEE, 2021.
- [25] Waqar Ahmad, Hilal Tayara, and Kil To Chong. Attention-based graph neural network for molecular solubility prediction. *ACS omega*, 8(3):3236–3244, 2023.
- [26] Tong Deng and Guo-zhu Jia. Prediction of aqueous solubility of compounds based on neural network. *Molecular Physics*, 118(2):e1600754, 2020.
- [27] Sumin Lee, Myeonghun Lee, Ki-Won Gyak, Sung Dug Kim, Mi-Jeong Kim, and Kyoungmin Min. Novel solubility prediction models: Molecular fingerprints and physicochemical features vs graph convolutional neural networks. *ACS omega*, 7(14):12268–12277, 2022.
- [28] David K Duvenaud, Dougal Maclaurin, Jorge Iparraguirre, Rafael Bombarell, Timothy Hirzel, Alán Aspuru-Guzik, and Ryan P Adams. Convolutional networks on graphs for learning molecular fingerprints. *Advances in neural information processing systems*, 28, 2015.
- [29] Sepp Hochreiter and Jürgen Schmidhuber. Long short-term memory. *Neural computation*, 9(8):1735–1780, 1997.
- [30] Ashish Vaswani, Noam Shazeer, Niki Parmar, Jakob Uszkoreit, Llion Jones, Aidan N Gomez, Łukasz Kaiser, and Illia Polosukhin. Attention is all you need. *Advances in neural information processing systems*, 30, 2017.
- [31] Ting Liu and Shu Lin. Comprehensive chemical characterization of qingkailing capsules by ultra-high-performance liquid chromatography combined with fourier transform ion cyclotron resonance mass spectrometry. *Separations*, 10(12):588, 2023.
- [32] Antonio Llinas, Ioana Oprisiu, and Alex Avdeef. Findings of the second challenge to predict aqueous solubility. *Journal of chemical information and modeling*, 60(10):4791–4803, 2020.
- [33] Patricio Cerda, Gaël Varoquaux, and Balázs Kégl. Similarity encoding for learning with dirty categorical variables. *Machine Learning*, 107(8):1477–1494, 2018.
- [34] Fuli Feng, Xiangnan He, Hanwang Zhang, and Tat-Seng Chua. Cross-gen: Enhancing graph convolutional network with k k-order feature interactions. *IEEE Transactions on Knowledge and Data Engineering*, 35(1):225–236, 2021.
- [35] Chengfeng Xu, Pengpeng Zhao, Yanchi Liu, Victor S Sheng, Jiajie Xu, Fuzhen Zhuang, Junhua Fang, and Xiaofang Zhou. Graph contextualized self-attention network for session-based recommendation. In *IJCAI*, volume 19, pages 3940–3946, 2019.
- [36] James Bergstra, Rémi Bardenet, Yoshua Bengio, and Balázs Kégl. Algorithms for hyper-parameter optimization. *Advances in neural information processing systems*, 24, 2011.
- [37] Christine A Frederick, Loren Dean Williams, Giovanni Ughetto, Gijs A Van der Marel, Jacques H Van Boom, Alexander Rich, and Andrew HJ Wang. Structural comparison of anticancer drug-dna complexes: adriamycin and daunomycin. *Biochemistry*, 29(10):2538–2549, 1990.
- [38] Thomas F Headen, Christopher A Howard, Neal T Skipper, Michael A Wilkinson, Daniel T Bowron, and Alan K Soper. Structure of π - π interactions in aromatic liquids. *Journal of the American Chemical Society*, 132(16):5735–5742, 2010.
- [39] A Martin, PL Wu, Z Liron, and S Cohen. Dependence of solute solubility parameters on solvent polarity. *Journal of pharmaceutical sciences*, 74(6):638–642, 1985.

- [40] Paul Ruelle and Ulrich W Kesselring. The hydrophobic effect. 2. relative importance of the hydrophobic effect on the solubility of hydrophobes and pharmaceuticals in h-bonded solvents. *Journal of pharmaceutical sciences*, 87(8):998–1014, 1998.
- [41] TJ Hou, Ke Xia, Wei Zhang, and XJ Xu. Adme evaluation in drug discovery. 4. prediction of aqueous solubility based on atom contribution approach. *Journal of chemical information and computer sciences*, 44(1):266–275, 2004.
- [42] Bradley D Anderson, J Howard Rytting, and Takeru Higuchi. Solubility of polar organic solutes in nonaqueous systems: role of specific interactions. *Journal of Pharmaceutical Sciences*, 69(6):676–680, 1980.
- [43] Babiker M El-Haj, Samrein BM Ahmed, Mousa A Garawi, and Heyam S Ali. Linking aromatic hydroxy metabolic functionalization of drug molecules to structure and pharmacologic activity. *Molecules*, 23(9):2119, 2018.